Electronic Supplementary Material (ESI) for Sustainable Energy & Fuels.

Supplementary Information For:

Evaluation of Flow Schemes for Near-Neutral pH Electrolytes in Solar-Fuels Generators

Meenesh R. Singh, Chengxiang Xiang*, and Nathan S. Lewis*

1. Physical Dimensions, Parameters, and Properties used in the Simulations

Table 1 shows the physical dimensions of the photoelectrochemical cell (PEC) in Figure 1. The cell dimensions are similar to the electrochemical cell in Ref. (1).

Table 1: Physical dimensions of a 1-D PEC.

Physical Description	Values (mm)
Electrode Spacing	8.2
Membrane Thickness	0.2
Boundary Layer Thickness	0.1
Electrode Width	37
Electrode Height	37

Table 2 shows the dimensions of a 2-D PEC, which has the mean ionic path length and flow-field similar to the 1-D PEC. The photoelectrode width of 18 mm yields the mean ionic path length of ~8.2 mm, which is the electrode spacing in 1-D PEC. The reported optimal value for membrane width is 10% of the half-width of the photoelectrochemical cell, which is ~ 1 mm.[2] The height of electrolyte in the 2-D photoelectrochemical cell is set to be equal to the width of electrolyte in the 1-D planar cell to ensure a similar flow field.

Table 2: Physical dimensions of a 2-D PEC.

Physical Description	Values (mm)
Electrolyte Height	4
Electrode Width	18
Electrode Height	0.1
Membrane Width	1
Membrane Height	0.1

Table 3 shows the electrolyte composition used in the computational studies. The polarization losses decrease with increasing buffer concentration.[3] However, increasing the buffer concentration above 0.5 M can favor crystallization of electrolyte at the electrode due to electrodialysis.[3] We have shown in the previous study that the buffer concentration of 0.5 M at pH 7.21 can be optimal to maintain pH near the electrodes at 10 mA cm^{-2} of current density.[3]

Table 3: Electrolyte composition used in the simulations

Species	Concentration (M)
Na^+	1.5
$H_2PO_4^-$	0.5
HPO_4^{2-}	0.5
H^+	$1 \times 10^{-7.21}$
OH^-	$1 \times 10^{-6.79}$

Table 4 shows the diffusion coefficients of species,[4] solubilities of gases[5] and pK_a of buffer and water. The diffusion coefficients of species are assumed for an infinitely dilute electrolyte at 25 ^oC.[4]

Table 4: Physical properties of electrolyte [4, 5]

Properties	Values
Diffusion Coefficient of Na^+	1.334×10^{-9} (m^2 s^{-1})
Diffusion Coefficient of $H_2PO_4^-$	0.879×10^{-9} (m^2 s^{-1})
Diffusion Coefficient of HPO_4^{2-}	0.439×10^{-9} (m^2 s^{-1})
Diffusion Coefficient of H^+	9.311×10^{-9} (m^2 s^{-1})
Diffusion Coefficient of OH^-	5.273×10^{-9} (m^2 s^{-1})
pKa of Phosphate Buffer	7.21
pKa of Water	14
Temperature	298 K
Solubility of H_2	0.78 mM
Solubility of O_2	1.23 mM
Diffusion Coefficient of H_2	4.5×10^{-9} (m^2 s^{-1})
Diffusion Coefficient of O_2	2.1×10^{-9} (m^2 s^{-1})

Table 5 shows diffusion coefficients of species, pK_a of buffer and water in the cation-exchange membrane. We have assumed that the pK_a of buffer and water does not change in the membrane. The cation-exchange membrane was modeled as an electrolyte with 1.0 M of background negative charges. The diffusion coefficients of cations were reduced by a factor of 10 [6] and that of anions were reduced by a factor of 100 [7, 8] relative to those for cations and anions, respectively, in the liquid electrolyte. The diffusion coefficients of O_2 [9]and H_2 [10] were obtained for a Nafion membrane.

Table 5: Physical properties of the cation-exchange membrane[6-10]

Properties	Values
Diffusion Coefficient of Na^+	1.334×10^{-10} (m^2 s^{-1})
Diffusion Coefficient of $H_2PO_4^-$	0.879×10^{-11} (m^2 s^{-1})
Diffusion Coefficient of HPO_4^{2-}	0.439×10^{-11} (m^2 s^{-1})
Diffusion Coefficient of H^+	9.311×10^{-10} (m^2 s^{-1})
Diffusion Coefficient of OH^-	5.273×10^{-11} (m^2 s^{-1})
pKa of Phosphate Buffer	7.21
pKa of Water	14
Temperature	298 K
Diffusion Coefficient of H_2	2.08×10^{-9} (m^2 s^{-1})
Diffusion Coefficient of O_2	0.82×10^{-9} (m^2 s^{-1})

Table 6 shows the kinetic parameters for the OER and HER, which were obtained by fitting the experimental current density versus voltage data for IrOx[11] and Pt,[12] respectively.

Table 6: Kinetic parameters for OER and HER[11, 12]

Physical Description	Values
Exchange Current Density for OER	1.4×10^{-4} (mA cm^{-2})
Anodic Transfer Coefficient for OER	1.0
Cathodic Transfer Coefficient for OER	0.1
Exchange Current Density for HER	1 (mA cm^{-2})
Anodic Transfer Coefficient for HER	2.57
Cathodic Transfer Coefficient for HER	2.57

Table 7 shows the physical parameters used for calculation of the pumping power requirements for Schemes A, B, and C. The physical dimensions of cell were taken from Table 1, the diameter of inlet and outlet ports was assumed to be 4 mm, and the density and viscosity of phosphate buffer were obtained for the composition of electrolyte given in Table 3.

Table 7: Parameters for calculation of pumping power requirement

Parameters	Values
Height of Electrode, H_{el}	37 (mm)
Width of Electrolyte, W_{el}	4 (mm)
Depth of Electrolyte, D_{el}	37 (mm)
Area of Inlet/Outlet Duct, A_d	12.56 (mm^2)
Density of Phosphate Buffer, ρ	1.064 (gm ml^{-1})
Viscosity of Phosphate Buffer, ν	1.05 (cP)

2. Computational Details

The mathematical model and computational scheme to obtain the species and potential distributions in 1-D and 2-D electrochemical cells are given in Singh et al.[3] and Jin et al.[13], respectively. We have used COMSOL Multiphysics to solve the Nernst-Planck equations coupled with Butler-Volmer equations for surface reactions with the Navier-Stokes equation for convection. The Galerkin FEM with linear elements were used to discretize the equations, which were solved using a Multifrontal Massively Parallel sparse direct Solver (MUMPS) with an adaptive Newton's method. The tolerance was set to $1x10^{-5}$, and the dependent variables were normalized based on their initial values. Approximately 50,000 triangular mesh elements were used to discretize the domain. This approach was optimized for the parameters considered in this study.

We have developed a 2-D computational model for the cells shown in Figure 1, where the electrolyte flow is along the length of electrodes and the diffusion and migration fluxes are perpendicular to the electrodes. This is effectively a 1-D transport as the species concentrations do not vary along the length of the electrodes. We have assumed a fully-developed laminar flow at the entrance of the electrochemical cells in Figure 1, as the entrance effect is negligible for electrode length > > 1mm. The height, width, and spacing of electrodes affects the volumetric exchange of electrolytes between anode and cathode in the recirculation flow Schemes -A and -B.

3. Effect of Variation in Diffusion Coefficients on the Polarization Losses

Figure S1 shows the decrease in the polarization loss with increasing diffusion coefficients. The polarization loss is calculated for the Scheme-A at the operational current density of 10 mA cm^{-2} and for a recirculation flowrate of 43.8 µl cm^{-2} min^{-1}. The polarization loss is ~83 mV for the diffusion coefficients of phosphate buffer species (shown at the 1X point in Figure S1). The polarization loss decreases to ~34 mV as the diffusion coefficients of phosphate buffer species increased fourfold (shown at the 4X point in Figure S1). The polarization loss increases to ~193 mV as the diffusion coefficients decreased twofold (0.5X point in Figure S1).

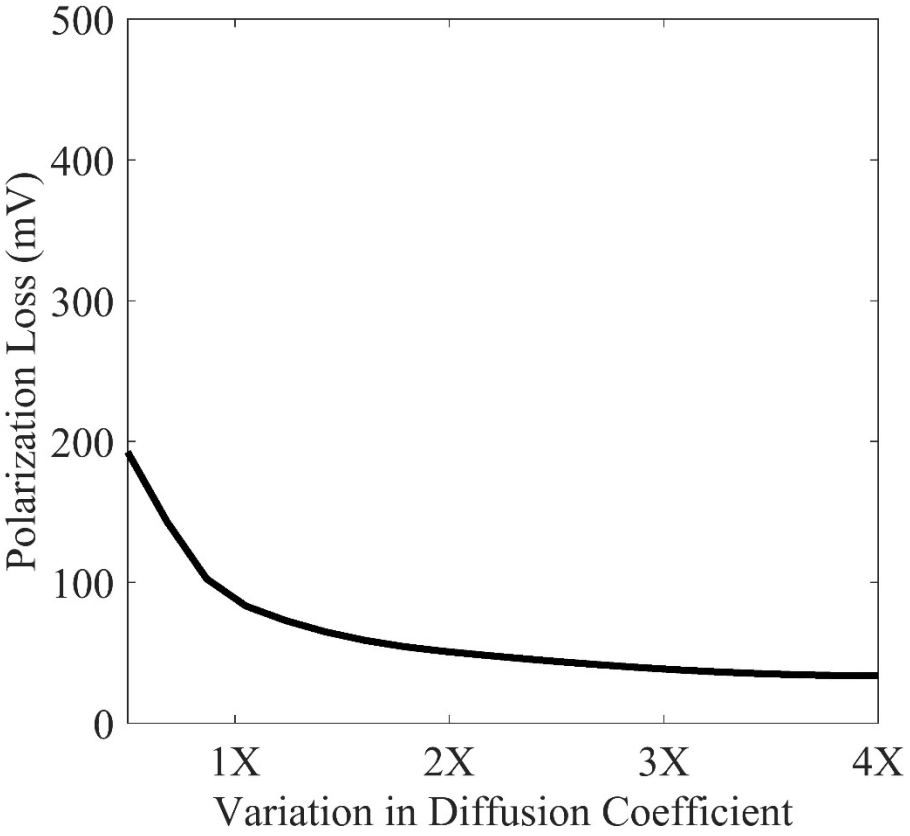

Figure S1: Polarization loss decreases with increasing diffusion coefficient of all species in the Scheme-A at the operational current density of 10 mA cm^{-2} and recirculation flowrate of 43.8 µl cm^{-2} min^{-1}. The x-axis corresponds to the number of folds of increase in the diffusion coefficient of the phosphate buffer species.

4. Gas-Crossover in Recirculation Cells

Figure S2 shows the percentage of gas-crossover flux due to recirculation. The percentage of H_2 in the O_2 product stream and O_2 in the H_2 product stream increases with increasing recirculation flowrates. Flammable gas mixtures of composition > 4.65%[14] H_2 in O_2 product stream can be produced at recirculation flowrates > 80 µl cm^{-2} min^{-1}.

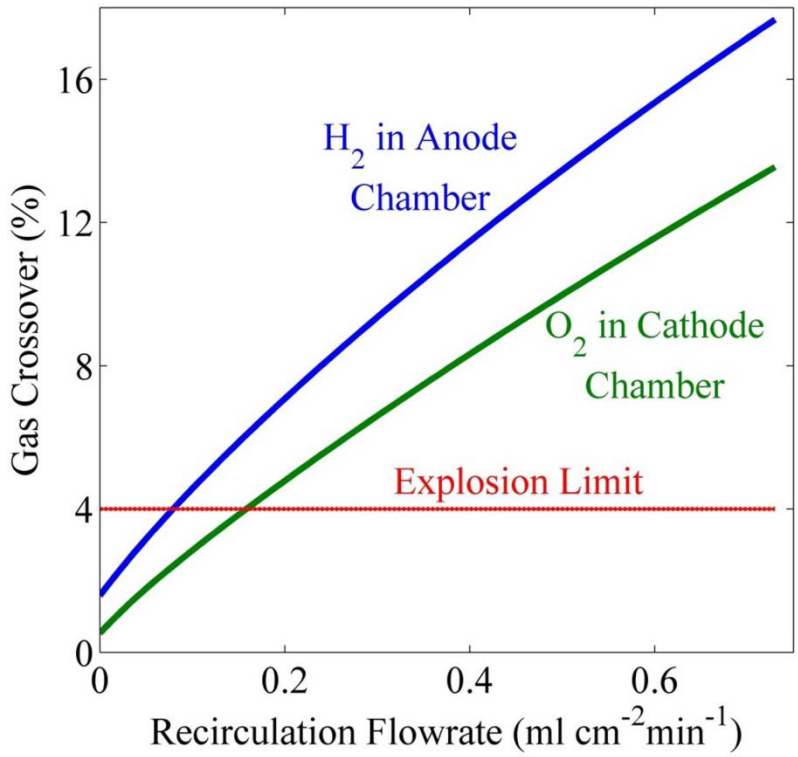

Figure S2: Percentage crossover of product gasses in the opposite chambers through membrane diffusion and convective transport as a function of recirculation flowrates. Flammable gas mixtures are produced at recirculation flowrates > 0.08 ml cm^{-2} min^{-1}. Operating conditions: pH 7.21, 0.5 M NaH_2PO_4 and 0.5 M Na_2HPO_4, 10 mA cm^{-2} current density, 8.2 mm electrode spacing, 0.2 mm membrane thickness and 0.1 mm boundary layer thickness (for Scheme-A)

5. Effect of Boundary Layer Thickness on the Polarization Losses

Previous computational studies have shown that the polarization losses increase with as the boundary-layer thickness in the stagnant photoelectrochemical cell increases.[3] Figure S3 shows the polarization losses due to the pH gradient as a function of the operating current density for Scheme A with a recirculation rate of 43.8 µl cm^{-2} min^{-1} and for a boundary-layer thickness of 50 µm, 100 µm, or 150 µm. At the operational current density of 10 mA cm^{-2}, the polarization losses for the boundary-layer thickness of 50 µm, 100 µm, and 150 µm were 4.13 mV, 9.01 mV, and 13.35 mV, respectively.

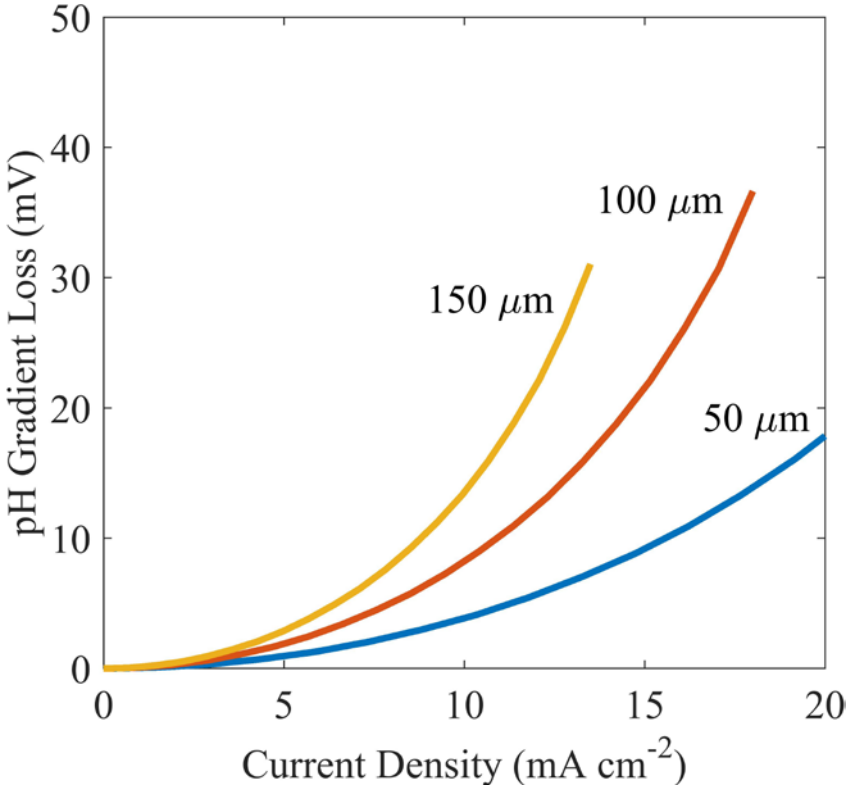

Figure S3: pH gradient loss versus current density for Scheme A operating at the recirculation rate of 43.8 µl cm^{-2} min^{-1} and the boundary-layer thickness of 50 µm, 100 µm, and 150 µm.

6. Important Factors for Implementation of Flow-cells

To produce cost-competitive hydrogen, pre-pressurization or electrochemical pressurization is often required.[15] Electrochemical pressurization of hydrogen can be readily achieved by, and robust gas separation and electrolyte transport are generally characteristic of, electrolyzers constructed using passive transport devices that operate at extreme pHs. The flow devices, in turn, will face significant engineering challenges in gas and fluid handling to produce and collect pressured H_2(g) that will affect the balance of systems design and cost. These factors must be considered in the future analysis and implementation of flow cells.

References

1. M. A. Modestino, K. A. Walczak, A. Berger, C. M. Evans, S. Haussener, C. Koval, J. S. Newman, J. W. Ager and R. A. Segalman, *Energy Environ. Sci.*, 2013, **7**, 297-301.
2. S. Haussener, C. Xiang, J. M. Spurgeon, S. Ardo, N. S. Lewis and A. Z. Weber, *Energy & Environmental Science*, 2012, **5**, 9922-9935.
3. M. R. Singh, K. Papadantonakis, C. Xiang and N. S. Lewis, *Energy & Environmental Science*, 2015, **8**, 2760-2767.
4. M. Flury and T. F. Gimmi, *Methods of Soil Analysis: Part 4 Physical Methods*, 2002, 1323-1351.
5. E. Wilhelm, R. Battino and R. J. Wilcock, *Chemical reviews*, 1977, **77**, 219-262.
6. Z. Samec, A. Trojanek and E. Samcova, *The Journal of Physical Chemistry*, 1994, **98**, 6352-6358.
7. A. Herrera and H. Yeager, *Journal of The Electrochemical Society*, 1987, **134**, 2446-2451.
8. K.-L. Huang, T. M. Holsen and J. R. Selman, *Industrial & engineering chemistry research*, 2003, **42**, 3620-3625.
9. C. M. Evans, M. R. Singh, N. A. Lynd and R. A. Segalman, *Macromolecules*, 2015, **48**, 3303-3309.
10. Z. Ogumi, T. Kuroe and Z. i. Takehara, *Journal of the Electrochemical Society*, 1985, **132**, 2601-2605.
11. C. C. McCrory, S. Jung, J. C. Peters and T. F. Jaramillo, *Journal of the American Chemical Society*, 2013, **135**, 16977-16987.
12. S. Trasatti, *Journal of Electroanalytical Chemistry and Interfacial Electrochemistry*, 1972, **39**, 163-184.
13. J. Jin, K. Walczak, M. R. Singh, C. Karp, N. S. Lewis and C. Xiang, *Energy & Environmental Science*, 2014, **7**, 3371-3380.
14. H. F. Coward and G. W. Jones, *Limits of flammability of gases and vapors*, DTIC Document, 1952.
15. J. A. Turner, *Science*, 2004, **305**, 972-974.